BILINGUAL PUBLISHING CO.
Pioneer of Global Academics Since 1984

**Journal of Construction Research**
https://ojs.bilpublishing.com/index.php/jcr-b

ARTICLE

# Flexural Behavior of 3D Printed Concrete Beam with Fiber Reinforcement

**Ghassan K Al-Chaar[1*] Andrij Kozych[2]**

1.Structural Engineer at CERL, United States
2.US Army Construction Engineering Corp, United States

ARTICLE INFO

*Article history*
Received: 20 January 2021
Accepted: 2 March 2021
Published Online: 30 March 2021

*Keywords*:
3D printing
Large scale
Basalt rebar
Aramid mesh
Flexure strength
Concrete
Warren truss

ABSTRACT

3D printing with concrete is a promising new method for rapid, low cost construction. The flexural strengths for reinforced/unreinforced and 3D printed/cast concrete Warren trusses were tabulated and the failure mechanisms were reported. The types of reinforcement used were rebar(basalt and steel), and mesh (basalt and aramid). The effect of loading geometry and loading speed was measured for basalt mesh and aramid mesh composite, respectively. Due to the expected variation in flexure between samples, it cannot be said whether small differences for various tests are significant. Variation stems from a microscopically uneven surface and random inhomogeneities in the bulk of the tested material which act as a microcrack catalyst and propagator. Since the tested beams are short specimens the numerical findings of other studies will vary based on the intended design. This paper is intended to assess the performance of various reinforcements in a qualitative sense by comparing basalt reinforcement with other reinforcements. It was found that cast beams tolerated deflection better but had a similar flexure strength compared as the printed beams. The steel and basalt rebar reinforced beams had the highest flexure strengths where the traditional steel rebar reinforcement outperformed the basalt in flexure by 36% and the basalt outperformed the steel in deflection by 40%. The basalt mesh outperformed the cast and printed unreinforced bars by a small margin but had only 25% of steel rebars' deflection at maximum flexure strength. The aramid mesh tolerated the biggest deflection out of any sample at 2.26 cm.

## 1. Introduction

### 1.1 Materials and Geometry

Concrete is one of the best construction materials around due to its mechanical performance, durability and economy. The addition of gravel boosts strength and shrinkage resistance and has the added benefit of low cost and availability near construction sites. Concrete without gravel is considered to be mortar (cement + aggregates) and cannot be used in primary structural members. The geometry to be manufactured was picked to be the warren girder truss (Figure 2) as it minimizes local tensile stresses and maximizes axial compressive stresses on the internal members.

**Corresponding Author:*
*Ghassan K Al-Chaar,*
*Structural Engineer at CERL, United States;*
*Email: ghassan.k.al-chaar@usace.army.mil*



DOI: https://doi.org/10.30564/jcr.v2i2.2823

### 1.2 3D Printing cement Literature Background

3D printing, aka additive manufacturing (AM), is a relatively new and powerful tool which stems from the original three-dimensional printer, also known as stereolithography apparatus, invented by Charles Hull in 1986 (Hull 1986). First used for rapid and cost-effective prototyping using an extruded plastic filament, this technology has evolved to produce novel components (impossible to fabricate with traditional subtractive manufacturing) with an increasing variety of materials, across a variety of industries. One of these materials is cement and will be the focus here.

Vertical 3D printing of various types of concrete has been done before on small (mm) and large (building size) scale [1-5]. Additive manufacturing of cements started in the late 90s [2], several years after additive manufacturing with plastic was developed. Multiple methods of AM cement have been developed, the two most notable being methods [1,2] similar to selective laser sintering (SLS), and sprayed concrete [3,4,10]. SLS utilizes a deposited, blanket layer of bulk material that is selectively fused together with a laser to produce a desired shape, layer by layer [11]. Gibbons 2010 [1] used a selective activation of a binder present in the bulk material. The binder was rapid hardening Portland cement along with organic modifiers for flowability and the deposited activating agent was water. Pegna 1997 [2] took a similar route and used sand as the bulk material and ordinary Portland cement as the selectively deposited material. The sprayed concrete will be the manufacturing method for this paper. This is where the concrete is mixed, pumped, and then extruded through a nozzle. More relevant works have focused on the large scale (>1m), fully automated manufacture of structural components using cement and other materials [3], as well as optimizing the rheology of a printable concrete with good flowability and a longer workability time, yet low slumping [4]. These variables are at odds with one another since a high viscosity cement will not slump much but may extrude with difficulty or not at all. Mechtcherine 2018 [10] tested the mechanical properties of 3D printed steel rebar with CEM 1 52.5 Portland cement and cementitious additives fly ash and silica fume as the matrix. Bos 2017 [13] developed a printing head that autonomously deposits reinforcement in the form of a steel wire into an unspecified concrete mix and Asperone (2018) [14] 3D printed a 3 meter long curved, truss beam which was manually reinforced with steel cables after printing.

This work [13, 14] on the flexural properties of steel reinforced, 3D printed beams comes closest to the scope of this paper, which uses a proprietary cement mix [12] and basalt and aramid reinforcement and tests the flexure behavior of a large scale (1.5 m) warren truss.

Mechanical testing of larger samples intrinsically leads to a higher variation between samples due to a larger number of critical defects and a greater potential for uneven loading conditions. For example, flexure for printed, unreinforced, truss = 327psi +/-73.6, CI=95%, σ=65.1, n=3. Therefore, the objective of this study is to qualitatively characterize the stress/strain behaviors of several cement composites and determine whether they are good candidates for future research and development.

## 2. Materials and Methods

### 2.1 Reinforcements

The challenge of automating the incorporation of reinforcement into printed concrete is an on-going study [3]; at this point, steel rebar, basalt fiber reinforced polymer (BFRP) bar, or basalt fiber reinforced polymer (BFRP) mesh between layers during printing has been placed manually. Steel rebar was chosen because it is standard and well understood reinforcement. BFRP bar and mesh were chosen because of their chemical and thermal resistance and as well as the global availability [8]. Finally, aramid, a class of material which includes Kevlar, was chosen because of its high strength, heat resistance, and military availability [6]. In an effort to understand the performance of 3-D printed concrete beams, an experimental study was carried out on beams of various reinforcement details such as steel, basalt fiber reinforced polymer, aramid mesh (1", 25.4mm), and basalt mesh (0.25", 6.35mm). The flexural capacities of beams, layered concrete, design configuration, and various reinforcements are explored.

### 2.2 Concrete [12]

It should be noted that other efforts [4, 10] at large scale 3D printing used similar mixtures to the one used here which had the following ingredients in common; Type 1 cement, a fine sand aggregate, fly ash and fumed silica additives, and one or more organic components (to control rheology).

The printed beams in this study all used a concrete mixture consisting of Type I cement, fine aggregate (sand), and coarse aggregate (sand) at a ratio of 1 : 2.3 : 1, respectively. The aggregates used were equal amounts of fine sand, coarse sand, and gravel. In order to maintain flowability from the nozzle, the coarse aggregate size (gravel) was limited to 3/8 inch. Dry additives (fly ash, silica fume, and bentonite clay) were added to adjust for the flowability, strength, and shape stability required by printable concrete. Strength development and rheological

 DOI: https://doi.org/10.30564/jcr.v2i2.2823

parameters were further targeted by the addition of liquid admixtures (EUCON 1037 plasticizer, BASF MasterMatrix33 rheology controller, and BASF FP 20 accelerator). This mix gives a strength of about 41.4 MPa at 28 days.

### 2.3 3D Printer

**Figure 1.** Picture of the 3D printer used

The printer was about 1.83 m by 3.35 m and 2.44 m high with a nozzle diameter 3.18 cm. The printer deposited the outer wall layer, then the diagonal infill. If reinforcements are used in the print, they are placed on a fresh layer of cement. The printer is then restarted to deposit the second layer, and process is repeated, as necessary.

### 2.4 Printing Challenges

There are three challenges with implementing this technology that will be discussed here: using adequate gravel as the reinforcement, printing horizontally, and placement of reinforcement. Printing a safe building using concrete is possible but special considerations must be taken into account when printing roof sections acting as slabs or beams. The lack of a support structure means the roof sections must be printed vertically on the ground, and then set into place by crane or a similar instrument once they have cured. Additionally, the gravel aggregate used must be smooth in order to minimize friction in the hose and nozzle opening. Finally, the reinforcements used here cannot be extruded out the printer. For this study, they were placed manually. This problem can be solved with the use of an additional robot for a more fully automated print job.

### 2.5 Specimen Preparation and Experimental Set-Up

Eight 1.52 m short beams were printed using the concrete mix designed to maintain flowability, strength, and shape stability. Two beams of similar cross section were casted for comparison with the printed beams. The geometry of printed and cast beams followed the simple Warren Girder truss design (Figure 2). In this case, the contiguous triangular truss that are usually made of timber, iron, or steel case are made of layered or cast concrete.

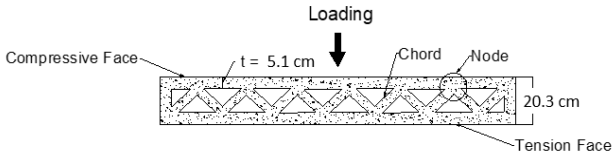


**Figure 2.** Typical Side View of Beam Sample that Mimic Warren Girder Truss

Printed specimens used a proprietary concrete [12] with different reinforcement including rebar and mesh. The reinforcements were placed manually between layer depositions while printing. Test Matrix are shown in Table 1. The concrete was also cast into forms as comparison between cast and printed beams as seen in Figure 3.

**Table 1.** Test Matrix*

| Specimen ID | Clear Span During Testing (m) | Reinforcement | Age of Specimens During Testing (day) | Weight of Specimen (kg) |
|---|---|---|---|---|
| **P.N.1** | 1.371 | None | 93 | 71 |
| **P.N.2** | 1.32 | None | 201 | 81 |
| **P.N.3** | 1.371 | None | 195 | 68 |
| **C.N.1** | 1.422 | None | 144 | 103 |
| **C.N.2** | 1.422 | None | 112 | 101 |
| **P.AM.1** | 1.371 | 1 Inch Mesh | 240 | 71 |
| **P.AM.2** | 1.32 | 1 Inch Mesh | 188 | 56 |
| **P.BM** | 1.371 | 0.25 Inch Mesh | 72 | 83 |
| **P.SR** | 1.371 | Steel rebar | 58 | 70 |
| **P.BR** | 1.371 | Basalt Rebar | 72 | 73 |

** Designation: P: Printed, C: Cast, N: None, AM: Aramid Mesh, BM: Basalt Mesh, SR: Steel Rebar, and BR: Basalt Rebar*



DOI: https://doi.org/10.30564/jcr.v2i2.2823

**Figure 3.** Oblique View of Cast (top) and Printed (bottom) Beams

Rebar reinforcement was only used in the tension side of printed beams and was evenly spaced to fit three across the width of each sample. Three layers of mesh reinforcements were placed across the entire beam width, parallel to the printed concrete plane. These configurations are illustrated in Figure 4.

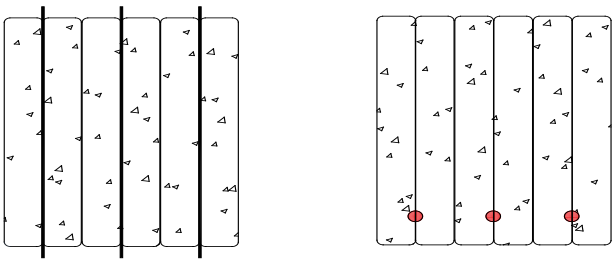

**Figure 4.** Cross Sections of Mesh Placement (left) and Rebar Placement (right)

Four point flexure strengths were determined according to ASTM C78 "Standard Test Method for Flexural Strength of Concrete"[5]. Printed samples were capped at four points where the loading arm contacts the beam using a sulfur compound to ensure even loading as shown in Figure 5. A ramp rate of 0.0254 cm/min. was used, loads were applied to failure 46 cm from both supports, and a clear span of 1.37 m was used.

**Figure 5.** Test apparatus for Testing Printed Concrete Beams

## 2.6 Reinforcement Properties

As shown in Figure 6, tensile strengths of #3 steel rebar (Grade 60), #3 basalt rebar, 2.54 cm. aramid mesh, and 0.635 cm basalt mesh were tested using the United Mechanical Testing Machine and software. Prepared materials were placed firmly within the grips of the machine and the tensile strength was recorded.

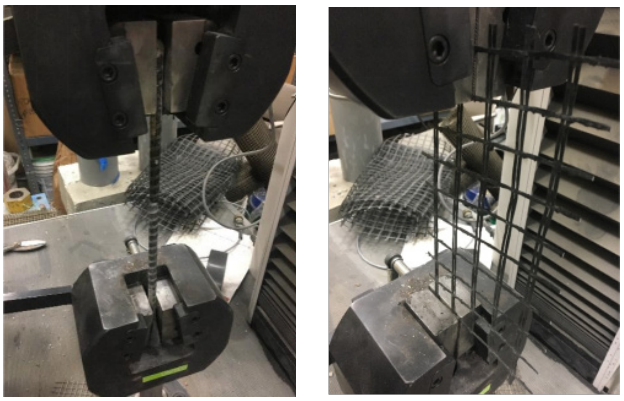

**Figure 6.** Experiment Set-up of Basalt Rebar (left) and Aramid Mesh (right)

Four #3 steel rebar tests were conducted. Typical mode of failure resulted in a steel rebar "cup-and-cone" configuration as shown in Figure 7, which indicates ductile fracture.

**Figure 7.** Cup-and-Cone Configuration

The average tensile strength of a #3 steel rebar was 621 MPa, above the 552 MPa minimum set by ASTM A615 for rebar of that grade. The #3 basalt rebar was tested and found to be reasonably close to the manufacturer's tensile strength of 1076 MPa. The tested 1 in. aramid mesh tensile strength was 862 MPa. The tested 0.635 cm basalt mesh failed at 1310 MPa. A summary of the results is shown in Table 2.


DOI: https://doi.org/10.30564/jcr.v2i2.2823

**Table 2.** Tensile Strength of Printed Beam Reinforcements

| Material | Average Tensile Strength (MPa) |
|---|---|
| # 3 Steel Rebar Grade 60 | 621 |
| # 3 Basalt Rebar | 1076 |
| 2.54 cm Aramid Mesh | 862 |
| 0.635 cm Basalt mesh | 1310 |

The stress-strain curves for the aramid and basalt mesh are shown in Figures 8 and 9.

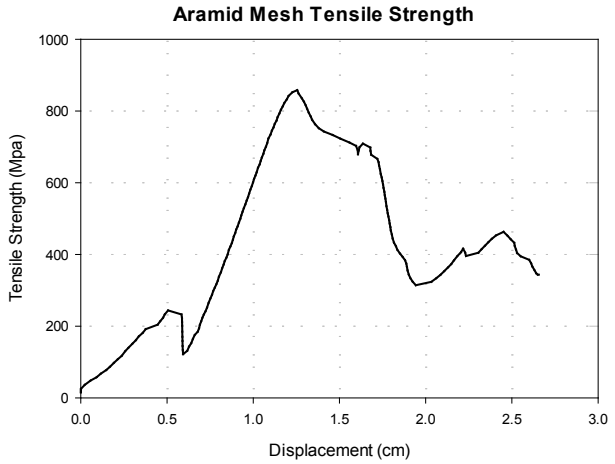


**Figure 8.** Stress-Strain Curve for Aramid Mesh

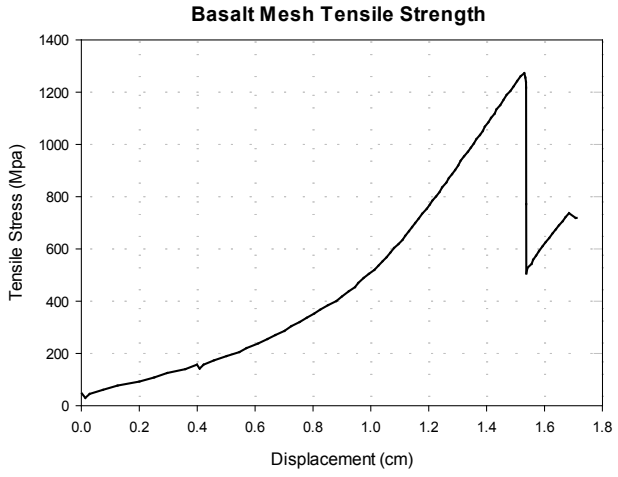


**Figure 9.** Stress-Strain Curve for Basalt Mesh

## 2.7 Calculation of Flexural Stresses

Because the samples are not simple boxes, assumptions had to be made to calculate flexure stress. Flexure stress was calculated as the product of the maximum moment, M, and the distance to the neutral axis from the free surface, y, divided by the moment of inertia, I, as shown below in Equation 1. The maximum bending moment is defined as the applied load multiplied by the length from load point to center, as shown in Equation 2.

$$\sigma_{Flexure} = My/I \qquad \text{Eq. 1}$$

$$M = \frac{PL}{6} \qquad \text{Eq. 2}$$

$$I = \frac{bh^3}{96} + \frac{bh^3}{176} + \frac{bh}{2}\left(\frac{3h}{4} - y\right)^2 + \frac{bh}{4}\left(\frac{h}{8} - y\right)^2 \qquad \text{Eq. 3}$$

| Where: | | |
|---|---|---|
| | M | Maximum Bending Moment |
| | y | Distance to Neutral Axis |
| | I | Moment of Inertia |
| | P | Applied Load |
| | L | Support Span |
| | b | Beam Width |
| | h | Beam Height |

The moment of inertia in Equation 3 uses the parallel axis theorem based on the geometry of Figure 10.

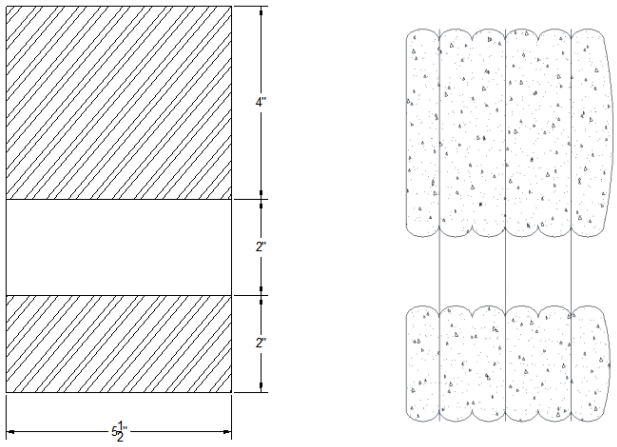


**Figure 10.** Asymmetric Cross-Section with Off-Centered Void Cast beam (Left), Printed Beam (Right)



DOI: https://doi.org/10.30564/jcr.v2i2.2823

## 3. Results

### 3.1 Flexure Strength and Deflection Results

Ten flexure tests were conducted such that all variables are controlled. The beams were designed such that the effect of one varied variable can be studied and compared qualitatively and quantitatively. Pairs of beams were compared as followed:

1.Performance of unreinforced printed beam versus cast beam

2.Performance of aramid mesh beams subjected to different load rates

3.Performance of beams reinforced with 2.54 cm Aramid and 0.635 cm Basalt Meshes

4.Comparison of Lateral and Vertical Loading on Basalt Mesh Beams

5.Comparison of printed beams reinforced with steel versus basalt rebar

The flexural strength of each specimen had to be adjusted for age, weight, and support span in order to provide an accurate comparison between beams. A support span of 1.37 m, an age of 28 days, and a weight of 72 kg were used as the basis of comparison. The results are shown in Table 3.

**Table 3.** Flexural Strength Adjustment

| ID* | Experimental Flexural Stress (MPa) | Span Correction Factor | Age Correction Factor | Weight Correction Factor | Corrected Flexural Stress (MPa) |
|---|---|---|---|---|---|
| P.N.1 | 1.89 | 1.00 | 0.91 | 1.01 | 1.74 |
| P.N.2 | 2.84 | 1.04 | 0.95 | 0.88 | 2.47 |
| P.N.3 | 2.55 | 1.00 | 0.95 | 1.05 | 2.55 |
| C.N.1 | 2.19 | 0.96 | 0.94 | 0.69 | 1.37 |
| C.N.2 | 3.23 | 1.00 | 0.93 | 0.71 | 2.14 |
| P.AM.1 | 1.47 | 1.04 | 0.96 | 1.01 | 1.48 |
| P.AM.2 | 2.23 | 1.00 | 0.95 | 1.28 | 2.71 |
| P.BM | 3.05 | 1.00 | 0.91 | 0.86 | 2.39 |
| P.SR | 8.12 | 1.00 | 0.85 | 1.03 | 7.12 |
| P.BR | 5.8 | 1.00 | 0.91 | 0.99 | 5.23 |

Span was adjusted using a correction factor determined by Equation 4.

$$\frac{L_1}{L_2} = \frac{\sigma_1}{\sigma_2} \quad \text{Eq. 4}$$

Where $L_1$ and $\sigma_1$ are the length and flexural strength of the experimental specimen respectively, and $L_2$ and and $\sigma_2$ is the length of the *basis* support span(54in, 137.2cm) and the corrected flexure strength is unknown. The correction factor is $L_2/L_1$ then.

The strength of concrete can increase over time. To account for this, an age reduction factor was calculated using a base age of 28 days, a compressive strength of 30 MPa, and Type I Concrete. Compressive strength (MPa) and slope (MPa/days) was estimated using Figure 3.7 in "Concrete 2nd Edition" (pg 28) [9].

Lastly, the weight correction factor is simply the ratio of average weight to actual weight. Note that the average weight excluded the weights of the two cast beams which are significantly heavier than the printed beams. To obtain the final adjusted flexural strength, the experimental flexural stress was multiplied by all three factors. The final results are shown in Table 4.

**Table 4.** Adjusted Flexure Strength and Deflection Results

| ID | Reinforcement | Maximum Load (kg) | Flexure Strength (MPa) | Deflection at Ultimate failure (cm) |
|---|---|---|---|---|
| P.N.1 | None | 585 | 1.74 | 0.25 |
| P.N.2 | None | 1184 | 2.47 | 0.28 |
| P.N.3 | None | 907 | 2.55 | 0.15 |
| C.N.1 | Cast | 1285 | 1.37 | 0.28 |
| C.N.2 | Cast | 1863 | 2.14 | 0.38 |
| P.AM.1 | 1" Mesh | 641 | 1.48 | 2.26 |
| P.AM.2 | 1" Mesh | 916 | 2.71 | 2.24 |
| P.BM | 0.25" Mesh | 1406 | 2.39 | 0.15 |
| P.SR | Steel Rebar | 3111 | 7.12 | 0.58 |
| P.BR | Basalt Rebar | 2434 | 5.23 | 0.81 |


DOI: https://doi.org/10.30564/jcr.v2i2.2823

### 3.1.1 Comparison of Unreinforced Printed and Cast Beams

As expected, the failure of unreinforced concrete, both cast and printed, occurred in between load points was always failure due to the lack of reinforcement in the tension section.

In this experiment, 3-D printed beams are expected to behave differently from cast beams due to limited interfacial bonding between layers and constrained reinforcement due to the size of the printer nozzle. The presence of surface flaws on an uneven, 3D printed surface served to initiate crack propagation and failure at a smaller deflection than compared to the cast specimen with a relatively smooth surface. The cast beams (C.N.1 and C.N.2) served as a comparison of the mechanical properties of a cast beam vs. a printed beam. The cast specimen reached a maximum average deflection of 0.28 cm at an average maximum stress of 2.7 MPa (corrected to 1.75 MPa). The 3-D-printed beams P.N.1 and P.N.2 were considered baseline beams as they contained no reinforcements. The printed specimen reached a maximum average deflection of 0.216 cm at stress of 2.55 MPa (corrected to 2.25 MPa). See Figure 11.

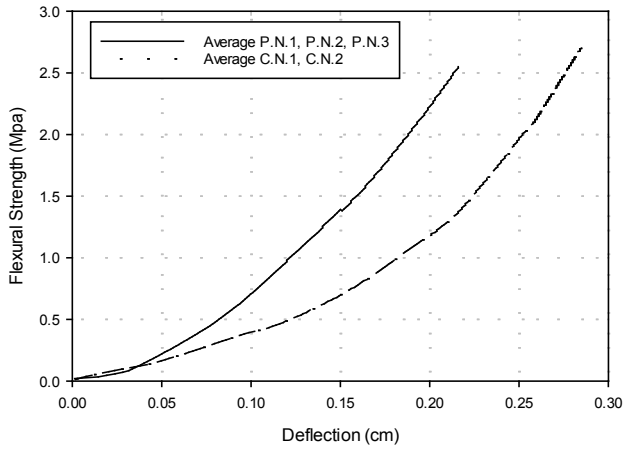


**Figure 11.** Comparison of Unreinforced Printed and Cast Beams

### 3.1.2 Comparison of Load Rates of Aramid Mesh Beams

P.AM.2 was loaded at a much quicker rate (0.0508 cm/sec) than P.AM.1(0.0254 cm/sec) resulting in a maximum, corrected stress of 2.71 MPa, which gives a maximum corrected stress about 1.8 times as much as that of P.AM.1. However, XX Zhang et. al [15] reported almost no difference for steel fiber reinforced cement loaded at rates of 3.3e-4 cm/s to 0.3 cm/s. This difference could be explained by running more tests and performing a statistical analysis as well as through modeling analysis which is not the scope of this paper. Results are shown in Figure 12.

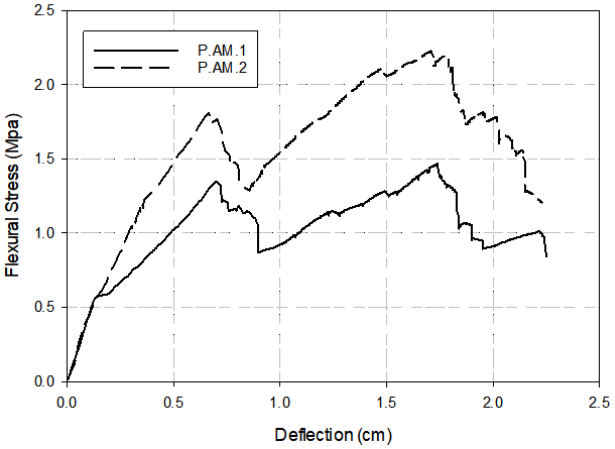


**Figure 12.** Comparison of Aramid Mesh Beams

### 3.1.3 Comparison of 2.54 cm Aramid and 0.635 cm Basalt Mesh

Beam P.AM.1 resulted in a large nonlinear region with a maximum deflection of 2.3 cm (about three times that of the basalt) and a maximum corrected stress of 1.48 MPa (about half of basalt max stress). This indicates a high degree of ductility in the aramid mesh as well as significant reduction in strength due to poor bonding between aramid and concrete. Beam P.BM reached a maximum corrected flexure stress of 2.39 MPa at a deflection of 0.15 cm. Beam P.AM.1 is able to retrain over 68% of its flexure strength after the maximum stress at 1.7 cm deflection which reveals some resistance to brittle failure after the maximum stress occurs. The tensile strength of the mesh also effected the stress and strain of the warren truss composite. As shown in Figure 13, the higher tensile strength (see Table 2) of the 0.635 cm basalt mesh resulted in increased flexural strength of the composite, but lower deflection than either component. This is likely due to a poor interfacial bond between the basalt mesh and the concrete. Besides this instance, we see that the stress/strain properties of the reinforcements serve to enhance and toughen the Warren truss composite. For example, the aramid mesh lowers the stress but greatly enhances the deflection of the composite, since it is a low stress/high deflection material on its own.



DOI: https://doi.org/10.30564/jcr.v2i2.2823

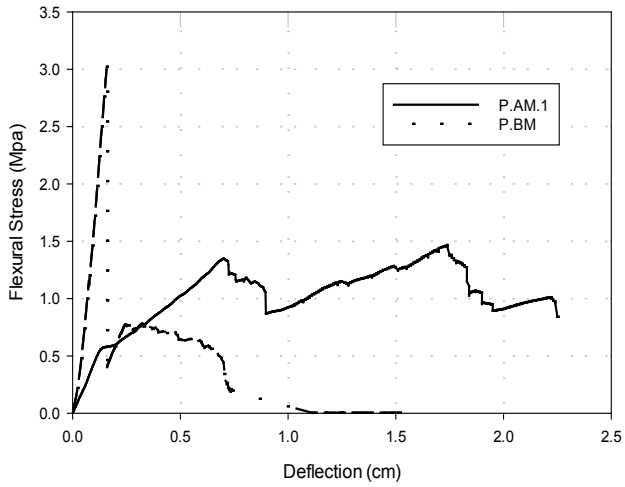


**Figure 13.** Comparison of 2.54 cm Aramid and 0.635 cm Basalt Mesh Samples

### 3.1.4 Comparison of Lateral and Vertical Loading on Basalt Mesh Beams

Basalt mesh was also subjected to lateral loading which may represent wind, seismic activity, etc. that the concrete slabs are exposed to. Testing the specimen both vertically and laterally allows for a bidirectional strength evaluation and a better understanding of the strength of the beam as a whole. Both beams underwent brittle failure, but the vertical loaded beam had a 20% greater maximum flexural stress than the lateral loaded one. The lateral beam had a maximum deflection of 1.75 cm and stress of 1.75 MPa. The significantly lower maximum stress value in comparison with the vertical load test can be attributed to the fact that the slabs are designed to have the highest flexural strength where it experiences the greatest load (in this case vertically). Stress-strain results for lateral and vertical loading are shown in Figure 14.

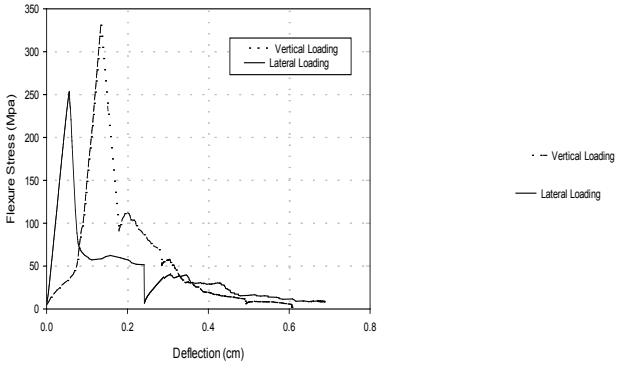


**Figure 14.** Stress-Strain Curves for Lateral and Vertical Loading of Basalt Mesh Composite

### 3.1.5 Comparison of Steel and Basalt Rebar

Beam P.SR reached a maximum deflection of 0.58 cm and stress of 7.0 MPa whereas beam P.BR reached a maximum deflection of 0.81 cm and stress of 5.2 MPa (Figure 15). Although the steel rebar composite produced a higher flexural strength, the lower maximum deflection reveals that this composite is more brittle compared with the BFRP bar. This is surprising given that steel rebar is weaker in tension than the BFRP bar and should, assuming rule of mixtures, yield at a lower stress. This observed behavior can be explained by poor bonding of the cement to the basalt rebar which also happens to explain the basalt mesh composite behavior. A poor bond would cause the basalt bars to delaminate from the concrete matrix and get pulled out under load, yet hold the bar together and prevent brittle failure, at least initially.

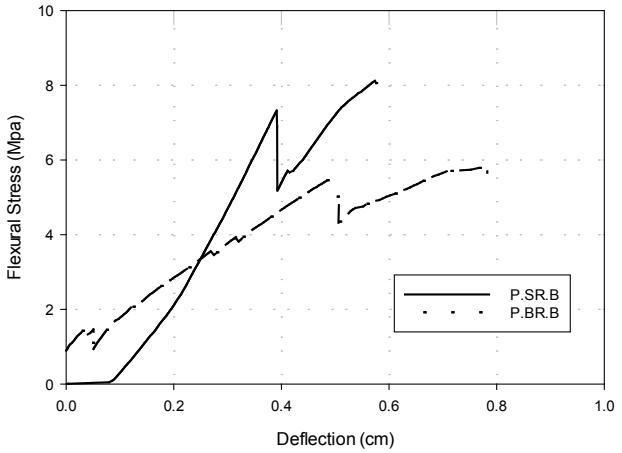


**Figure 15.** Comparison of Steel and Basalt Rebar

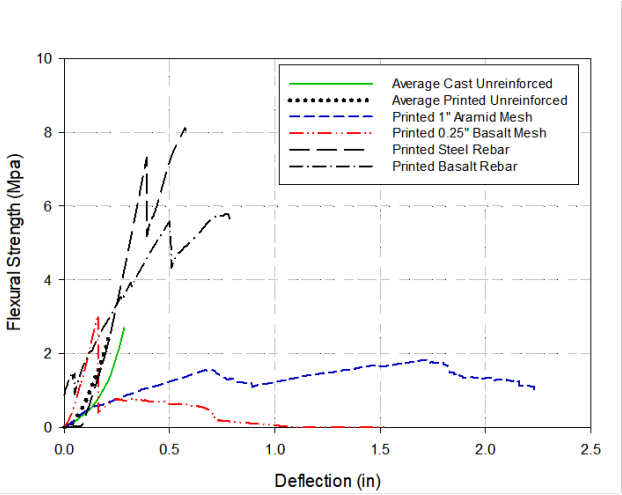


**Figure 16.** Summary of Flexure Strength, Maximum Deflection, and Reinforcement Type

A summary of flexural strengths, maximum deflections,

 DOI: https://doi.org/10.30564/jcr.v2i2.2823

and reinforcement types is shown in Figure 16. It was found that steel bar produced the highest flexural strength while BFRP bar was the toughest and was second highest in strength and second highest in deflection.

### 3.2 Modes of Failure

In all samples, excluding specimens with rebar reinforcement, the mode of failure consisted of a fracture occurring in the tension member near the center of the beams as shown in Figure 17.

**Figure 17.** Six Types of Beams That Were Tested to Failure by Four Point Bending: Cast (bottom), Unreinforced, 0.64 cm Mesh, 2.54 cm Mesh, 0.95 cm Basalt Rebar, 0.95 cm Steel Rebar (top)

Overall, the failure of reinforced concrete beams failed with higher deflections than the unreinforced beams resulting in nonlinear deformation beyond the ultimate flexural strength. The failure behavior of the cast and unreinforced printed beams was very similar; flexural cracks formed at the bottom core (tension side) of the beam and propagated upwards. However, in contrast to the cast beam, the top core of the printed beam failed in bending while the diagonal chords experienced shear failure. See Figure 18.

**Figure 18.** Failure of Printed (top) and Cast (bottom) Beams

For both aramid and basalt mesh, flexural cracks occurred between nodes and propagated in the tension side (bottom) of the beam as shown in Figure 19. Failure occurred the load was transferred from the concrete matrix to the fiber reinforcement, and the meshes underwent splitting (Figure 20). A comparison of the break sites of the 2.54 cm aramid mesh and 0.635 cm basalt mesh is shown in Figure 21.

**Figure 19.** Basalt Mesh Beam Before and After Loading and Crack Propagation

**Figure 20.** Basalt Mesh Splitting

**Figure 21.** Break Site of Aramid (left) and Basalt (right) Mesh



DOI: https://doi.org/10.30564/jcr.v2i2.2823

Lateral loading of the basalt mesh beam failed by flexural cracks occurring at the tension side (bottom) of the beam and propagating upwards towards the compression side (top) of the beam (Figure 22). The beam underwent mesh splitting similar to that of the vertically loaded basalt mesh beam and the aramid mesh beam.

**Figure 22.** Printed Basalt Mesh Beam Before and After Lateral Loading

Steel and basalt rebar composites broke outside of the support span as seen in Figure 23. This is due to the close proximity of the rebar to the free surface at the end, leading to surface spalling and eventual fracture. Failure occurred when the load was transferred from the concrete matrix to the rebar reinforcement. A comparison of the break sites of the steel and basalt-reinforced beams is shown in Figure 24.

**Figure 23.** Failure of Rebar-Reinforced Concrete

**Figure 24.** Break Site of Steel (left) and Basalt (right) Rebar

## 4. Discussion

### 4.1 Scalability

Larger concrete bodies have the tendency to have weaker macroscopic properties such as flexure strength, because the number of critical flaws is proportional to the sample volume. The size of test samples conducted herein is compared to smaller and larger samples. The equation below shows the theoretical proportionality of similar samples of different sizes.

Given support lengths $L_1$ and $L_2$

Given loads $P_1$ and $P_2$

Given Moments $M_1$ and $M_2$ If $M_1 = M_2$

Then $P_1L_1 = P_2L_2$

And $P_1 = (P_2L_2)/L_1$ Eq. 5

As a reminder, $P_1$ is the load applied at one of two load points in four-point bending. For example, if 45.4 kg is applied in four-point loading then $P_1$ would equal 22.7 kg. Similarly, $L_1$ is the distance between support point and load point. Again, for example, if the support span is 1.37 m then $L_1$ is equal to 1.37/3, or 0.46 m.

 DOI: https://doi.org/10.30564/jcr.v2i2.2823

### 4.1.1 1.52 m (5-Foot) Beam Comparison

For a 4.88 m wide roof panel, the distance between the support point at the wall and beam center where the weight is applied is 2.44 m. Using Equation 1, the maximum load before failure of a 4.88 m beam in three point bending is $3P_2/4.88$.

**Table 5.** 16 Foot (4.88 m) Beam Theoretical Maximum Loads Using 5 Foot (1.52 m) Beam Data

| Reinforcement Type | 1.52 m Load at Failure (Actual) kgs | 4.88 m Load at Failure (Theory) kgs |
|---|---|---|
| No Reinforcement | 1184 | 222 |
| Unreinforced Cast | 1285 | 240 |
| 2.54 cm Aramid Mesh | 916 | 172 |
| 0.635 cm Basalt Mesh | 1406 | 263 |
| 0.95 cm Basalt Rebar (Tension) | 2434 | 456 |
| 0.95 cm Steel Rebar (Tension) | 3111 | 583 |

If steel reinforced composites were used as roof panels, the theoretical maximum weight before failure is 583 kgs.

### 4.1.2 4.88 Meter (16 foot) Beam Comparison

**Table 6.** 4.88 m Beam Theoretical Maximum Loads (3 Point) Using 4.88 m Beam Data (4 Point)

| Reinforcement Type | 4.88 m Beam Load at 4 Point Failure (Actual) lbs | 4.88 m Beam Load at 3 Point Failure (Theory) lbs |
|---|---|---|
| Tension Steel Rebar | 1306 | 816 |
| T/C Rebar, No Mesh | 1524 | 952 |
| T/C Bas. Rebar, No Mesh | 812 | 508 |
| T/C Rebar Bas. Mesh | 1802 | 1127 |
| T/C Rebar Bas. Mesh | 1857 | 1161 |
| T/C Rebar Bas. Mesh (25.4 cm.) | 1974 | 1234 |

Four-point bending tests were also conducted on 4.88 m beams, as shown in Figure 2. The distance, $L_1$, between support point and load point was measured as 1.52 m for the 4-point test. Using Equation 1, the maximum load before failure of a 4.88 m roof panel in three-point bending is $1.52P_2/2.44$.

If steel reinforced composites with an increased height of 25.4 cm are used as roof panels, the theoretical maximum weight before failure is 1234 kgs. This is substantially larger than approximations using 1.52 m beam data.

## 5. Conclusions

Both printed and cast in place beams exhibited similar stresses. However, the printed beams tolerated less deflection than the cast beams by 23%. It was found that higher loading rate for the aramid mesh samples resulted in a 83% higher stress and a negligible difference in deflection.

Ultimate stress at vertical loading on a reinforced basalt mesh beam is higher by about ~36% compared with lateral loading due to the diagonal members distributing the applied load more effectively in the vertical direction.

While the basalt rebar is tougher than the steel rebar, it only reached 71% of steel's deflection before failure. This is likely due to the poor bonding of printed concrete with the basalt reinforcement since it was observed that the basalt rebar pulls out of the concrete and delaminates quite easily. Therefore, basalt rebar reinforcement is not as effective as the standard rebar reinforcement. More testing would be needed to confirm this hypothesis which could include a surface roughness characterization and/or fiber pullout mechanical tests.

The comparisons for flexure stress given here should not be taken exactly due to insufficient number of samples and the aforementioned high intrinsic variation of these samples.

## Author Contributions

The main author Dr. Al-Chaar contributed about 90% of the work from the proposed stage. He planned and executed the test matrix. He analyzed the date and drew conclusions. Mr. Kozych verified the data, updated graphs, and assisted in preparing this article.

## Funding

This study was conducted for U. S. Army, "Automated Construction of Expeditionary Structures." The technical monitor was Mr. Kurt J Kinnevan, CIV USARMY CEERD-CERL (USA).



DOI: https://doi.org/10.30564/jcr.v2i2.2823

## Acknowledgments

The work was performed by the Materials and Structural Branch of the Facilities Division, U.S. Army Engineer Research and Development Center, Construction Engineering Research Laboratory (ERDC-CERL).

## Conflicts of Interest

The authors declare no conflict of interest. The sponsors had no role in the design, execution, interpretation, or writing of the study.

## References

[1] G J Gibbons, R Williams, P Purnell & E Farahi (2010) 3D Printing of cement composites, Advances in Applied Ceramics, 109:5, 287-290, DOI:10.1179/174367509X12472364600878.

[2] Joseph Pegna, Exploratory investigation of solid freeform construction, Automation in Construction, Volume 5, Issue 5, 1997, Pages 427-437, ISSN 0926-5805, https://doi.org/10.1016/S0926-5805(96)00166-5.

[3] Khoshnevis, Behrokh. "Automated construction by contour crafting—related robotics and information technologies."Automation in construction 13.1 (2004): 5-19.

[4] Le, Thanh T., et al. "Mix design and fresh properties for high-performance printing concrete." Materials and structures 45.8 (2012): 1221-1232.

[5] ASTM C78 / C78M, 2016, "Method for Flexural Strength of Concrete (Using Simple Beam with Third-Point Loading)," ASTM International, West Conshohocken, PA, 2016, Available at: https://compass.astm.org/EDIT/html_annot.cgi?C78+18 [Accessed 23 Jul. 2019].

[6] DuPont (2017). Technical Guide: KEVLAR Aramid Fiber. [EBook] Richmond: DuPont. Available at: https://www.dupont.com/content/dam/dupont/products-and-services/fabrics-fibers-and-nonwovens/fibers/documents/Kevlar_Technical_Guide.pdf [Accessed 23 Jul. 2019].

[7] European Patent Office (2019). Method and apparatus for production of three-dimensional objects by stereolithography. EP0171069.

[8] Li, H., Xian, G., Xiao, B. and Wu, J. (2010). Comprehensive Characterization of BFRP Applied in Civil Engineering. Springer, Berlin, Heidelberg.

[9] Mindess, S., Young, J. and Darwin, D. (2008). Concrete. Taipei: Pearson Education Taiwan (p28).

[10] Mechtcherine, Viktor, et al. "3D-printed steel reinforcement for digital concrete construction–Manufacture, mechanical properties and bond behaviour." Construction and Building Materials 179 (2018): 125-137.

[11] ("Design Guide: Selective Laser SIntering (SLS) version 2.1," n.d.).

[12] Al-Chaar, G., Case, P., Northrop, G., Kreiger, M., n.d. Printable Concrete Composition. US patent Pub. No. 2018/0057405 A1.

[13] Bos, Freek P., et al. "3D printing concrete with reinforcement." High Tech Concrete: Where Technology and Engineering Meet. Springer, Cham, 2018. 2484-2493.

[14] Asprone, Domenico, et al. "3D printing of reinforced concrete elements: Technology and design approach." Construction and Building Materials 165 (2018): 218-23.

[15] X.X. Zhang, A.M. Abd Elazim, G. Ruiz, R.C. Yu, Fracture behaviour of steel fibre-reinforced concrete at a wide range of loading rates, International Journal of Impact Engineering, Volume 71, 2014, Pages 89-96, ISSN 0734-743X, https://doi.org/10.1016/j.ijimpeng.2014.04.009.

 DOI: https://doi.org/10.30564/jcr.v2i2.2823